Further Developments in Estimating Cloud Liquid Water over Land Using Microwave and Infrared Satellite Measurements

THOMAS J. GREENWALD, CYNTHIA L. COMBS, ANDREW S. JONES, DAVID L. RANDEL, AND THOMAS H. VONDER HAAR

Cooperative Institute for Research in the Atmosphere, Colorado State University, Fort Collins, Colorado

(Manuscript received 29 April 1996, in final form 10 September 1996)

ABSTRACT

Refinements and improvements of an earlier technique to retrieve the cloud liquid water path (LWP) of nonprecipitating clouds over land surfaces using Special Sensor Microwave/Imager (SSM/I) 85.5-GHz measurements are presented. These techniques require estimates of the microwave surface emissivity, which are derived in clear-sky regions from SSM/I measurements and window infrared measurements from the Visible and Infrared Spin Scan Radiometer on *GOES-7*. A comparison of forward model calculations with SSM/I measurements in clear regions demonstrates that over a 7-day period the surface emissivities are stable.

To overcome limitations in the single-channel retrieval method under certain situations, a new method is developed that uses a normalized polarization difference (NPD) of the brightness temperatures. This method has the advantages of providing estimates of the LWP for low clouds and being extremely insensitive to the surface skin temperature. Radiative transfer simulations also show that the polarization difference at 37 GHz may be useful for retrievals in high water vapor environments and for large cloud LWP.

An intercomparison of the different retrieval methods over Platteville, Colorado, reveals large discrepancies for certain cases, but the NPD method is found to agree best with coincident ground-based microwave radiometer measurements of cloud LWP. This success is primarily due to the larger than average surface polarization differences near the Platteville site. While the NPD method shows promise in distinguishing between low, moderate, and high values of cloud LWP, a comprehensive validation effort is required to further evaluate its accuracy and limitations.

1. Introduction

The use of passive microwave radiometry to retrieve cloud liquid water over land surfaces is an area of research that has been only modestly explored. A summary of past techniques is discussed by Jones and Vonder Haar (1990). More recently, simulation studies, such as those by Eyre (1990), Huang and Diak (1992), and Diak (1995), have been carried out to extract information about cloud properties, including cloud liquid water path (LWP), from microwave and, in some cases, infrared measurements.

Despite the progress achieved from these studies, there remains a widespread belief in (and outside of) the microwave remote sensing community that satellite instruments that measure microwave radiation at window frequencies, such as the Special Sensor Microwave/Imager (SSM/I), are largely incapable of observing cloud liquid water over land (e.g., Alishouse et al. 1990; Petty 1990; Wielicki 1995). The exploratory study of Jones and Vonder Haar (1990), however, concluded that the 85.5-GHz channels of the SSM/I showed promise in estimating cloud LWP over land surfaces. Much of their success was due to the larger cloud attenuation at 85.5 GHz and their ability to minimize the effects of surface emissivity variations. As will be shown, the results of this study reinforce the conclusions of Jones and Vonder Haar (1990) (hereafter JV90) and further demonstrate that the detection and retrieval of cloud liquid water over land surfaces is indeed feasible using the highest frequency channels of the SSM/I.

The remote sensing of cloud LWP over land has a number of important applications. For instance, cloud LWP might be useful as one indicator of the potential for aircraft icing. An ocean-based aircraft-icing index has been recently developed by Lee et al. (1994), which incorporates SSM/I observations of cloud LWP. In the context of global climate studies, satellite estimates of cloud LWP can also contribute to a better understanding of the connection between cloud physical properties and the radiation budget, which is important since clouds are known to have a significant impact on the radiation balance of the earth (Wielicki et al. 1995). This line of research has been explored by Zuidema and Hartmann (1995) and Greenwald et al. (1995) using SSM/I cloud

Corresponding author address: Dr. Thomas J. Greenwald, Cooperative Institute for Research in the Atmosphere, Colorado State University, Foothills Campus, Fort Collins, CO 80523.
E-mail: greenwald@cira.colostate.edu

LWP observations and Earth Radiation Budget Experiment measurements for low clouds over the oceans. Moreover, these observations will be useful in compiling climatic datasets of cloud LWP over land regions and serve as a source of validation for climate models that currently predict cloud liquid water (e.g., Fowler et al. 1996).

The main concern of this study is to extend and improve the method of JV90 to retrieve cloud LWP for nonprecipitating clouds over land surfaces using SSM/I measurements. Another aim is to investigate the retrieval problem more thoroughly—in particular, to identify potential problems and limitations. As in the method of JV90, we use 85.5-GHz measurements and rely on surface emissivity composites, which are created from near-coincident and collocated SSM/I measurements and window infrared measurements under clear sky conditions. The modified method introduced here takes advantage of a polarization difference of the brightness temperatures at 85.5 GHz.

In the following section the datasets used in this study are described. Section 3 involves an analysis of the SSM/I observations in regions of clear sky. In section 4 a simple demonstration is given of the ability of measurements at 85.5 GHz to detect cloud liquid water over land. This is followed by an overview of the difficulties inherent in over-land cloud liquid water retrievals. Section 6 describes the polarization difference method, and finally, a comparison of this new method to the previous single-channel approach is presented, with the aid of ground microwave measurements of LWP.

2. Region of study and data sources

A large sector of the western and central United States was chosen for this study, an area bounded from 95°W to about 105°W and from roughly 35°N to 45°N. The analyses were also limited to the months of August and September of 1991. The selection of this area and the specific time period was based on the availability of *GOES-7* data and the location of the ground microwave radiometer, which was near Platteville, Colorado. These ground data were used to independently evaluate the different retrieval methods in section 7. Over this 2-month period a total of 22 cases (i.e., satellite overpasses) were chosen.

The primary measurements used in this study originate from the SSM/I on the Defense Meteorological Satellite Program (DMSP) *F-10* satellite. The DMSP satellite flies in a near-polar orbit, with an inclination of 98.8°. The local equatorial crossing times for the DMSP *F-10* satellite are 0700 and 1942. The SSM/I is a dual-polarization radiometric system that passively senses radiation at 19.35, 22.235, 37, and 85.5 GHz. The instrument scans conically, with a constant zenith angle of 53.1°. The various channels of the SSM/I and their effective spatial resolutions are summarized in Table 1. A more detailed description of the SSM/I can be found in Hollinger et al. (1990).

TABLE 1. Selected Special Sensor Microwave/Imager instrument characteristics (Hollinger et al. 1990).

Channel number	Frequency (GHz)	Polarization (H or V)	Effective 3-dB field of view (km)
1	19.35	V	69 × 43
2	19.35	H	69 × 43
3	22.235	V	60 × 40
4	37.0	V	37 × 28
5	37.0	H	37 × 29
6	85.5	V	15 × 13
7	85.5	H	15 × 13

V—vertical.
H—horizontal.

Measurements are also used from the Visible and Infrared Spin Scan Radiometer (VISSR) onboard *GOES-7*. Of interest to this study are the visible channel (0.65 μm) and channel 8 (11 μm) measurements. Although data may also have been available from the Operational Line Scanner (OLS) on the DMSP satellite, *GOES-7* data were used since they were more convenient to obtain. The time of the *GOES-7* measurements is within 15 min of the DMSP overpass, with an average time differential of approximately 9 min.

Radiosonde data from the standard upper-air network and hourly surface measurements of the air temperature were also an integral part of the analyses. These data were used principally in the forward calculations for the clear-sky analysis and in the cloud liquid water retrievals.

Ground-based observations of cloud LWP were obtained from a microwave radiometer located in Platteville (40.18°N, 104.73°W). The dual-frequency radiometer is operated by the National Oceanic and Atmospheric Administration (NOAA) Environmental Technology Laboratory in Boulder, Colorado, and has frequencies at 20.6 and 31.6 GHz. The method used to retrieve cloud LWP and integrated water vapor simultaneously is described by Hogg et al. (1983). The data used here were integrated over a 2-min interval.

A powerful tool that was used in most aspects of the analyses to remap and collocate measurements from the different sensors was the data fusion method of Jones et al. (1995), also referred to as PORTAL (Polar Orbiter Remapping and Transformation Application Library). PORTAL was used to maintain the full resolution of the satellite measurements while reducing the overall computational requirements of the retrieval methods.

The microwave surface emissivities used throughout this study were determined from SSM/I observations and near-coincident *GOES-7* IR measurements for clear sky conditions, following the method described by JV90. Composites of surface emissivity over a 7-day period were created to provide a more complete spatial field. The validity of using these 7-day composites is discussed in the next section.

3. Clear-sky analysis

Before proceeding to the detection and retrieval of cloud liquid water over land, it is essential to first investigate the forward problem in regions of clear sky. Our ability to simulate the 85.5-GHz SSM/I measurements over land under clear sky conditions is important for several reasons. First, it can provide an indication of the integrity of the surface emissivity composites. Also, it gives us further confidence in attacking the inverse problem and can yield a quantitative measure of the anticipated background noise level above which retrievals can be performed.

From the 22 DMSP satellite overpasses described previously, *GOES-7* IR measurements were used to find SSM/I fields of views (FOVs) that were free of clouds. Only IR measurements were used in the cloud detection since visible measurements were not always available. The cloud detection method consisted of a simple threshold of the IR measurements (280 K or 290 K in combination with a standard deviation of greater than 1.5 K within the SSM/I FOV) along with a threshold of the difference between a spatially interpolated surface air temperature and the IR brightness temperature (5.5 or 8 K, depending on the situation). Inspection of the IR imagery revealed that the cloud-clearing method worked very well in most cases.

A transmittance form of the radiative transfer equation was used to compute the upwelling brightness temperature at the top of the atmosphere (TOA). The upwelling intensity at the TOA at frequency ν for vertical (V) or horizontal polarization (H) can be expressed as

$$I_{\nu,\mathrm{V/H}} = \epsilon_{\nu,\mathrm{V/H}} B_\nu(T_s)\tau_\nu + \int_{p_s}^{0} B_\nu[T(p)]\frac{\partial \tau_\nu(p,0)}{\partial p}\,dp + (1-\epsilon_{\nu,\mathrm{V/H}})\tau_\nu^2 \int_{p_s}^{0} \frac{B_\nu[T(p)]}{[\tau_\nu(p,0)]^2}\frac{\partial \tau_\nu(p,0)}{\partial p}\,dp + (1-\epsilon_{\nu,\mathrm{V/H}})\tau_\nu^2 B(T_{\cos}), \quad (1)$$

where ϵ is the surface emissivity, B_ν is the Planck function, T_s is the surface skin temperature, τ_ν is the total transmittance of the atmosphere, p is the pressure, p_s is the surface pressure, and $T_{\cos}$ is the cosmic background temperature. The first term in (1) is the emission from the surface attenuated by the atmosphere; the integral terms are the contributions from the atmosphere, including that reflected by the surface; and the last term is the radiation from space reflected by the surface.

The atmospheric transmittance was computed from Liebe's 1992 Millimeter-wave Propagation Model (MPM) (Liebe 1989; Liebe et al. (1993), using either the 0000 or 1200 UTC (whichever was closest in time to the DMSP overpass) humidity and temperature profiles from the upper-air network, interpolated via a Barnes objective analysis (Koch et al. 1983). To ensure that the surface emissivity composites were representative of the surface conditions, those locations that contained only one data point in the composite or had a standard deviation greater than 0.02 over the composite period were excluded from the comparison (standard deviations rarely exceeded 0.02 and were usually associated with small lakes). Absolute errors in the derived surface emissivities are estimated to be about 0.012 (JV90).

Figure 1 shows the predicted versus instantaneous SSM/I brightness temperatures (T_b's) at vertical and horizontal polarizations, separated into ascending and descending DMSP passes. In these calculations an interpolated surface air temperature (at the hour closest to the overpass) was used as an approximation for the skin temperature. Each data point represents an individual 85.5-GHz pixel.

The key point in Fig. 1 is the difference in the results between the ascending and descending passes, which suggests a diurnal effect. This behavior is likely caused by the surface air temperature lagging behind the skin temperature, the degree to which depends on a number of factors, including the level of water vapor, wind speed, and surface type (Minnis and Harrison 1984). Since the local time of the ascending pass of the DMSP *F-10* satellite occurs in the midmorning (0900–1000), the skin temperature is expected to be higher than the surface air temperature, thus causing the underestimation of the predicted values of the brightness temperatures seen in Fig. 1a,c. For the descending passes the behavior is just the opposite (Figs. 1b,d). The predicted values are biased higher than the observations by 1–2 K since the descending pass is in the early evening (2000–2100 LST) where the skin temperature will be lower than the surface air temperature.

These ideas can be tested by using actual skin temperatures in the calculations, as shown in Fig. 2. The skin temperatures were derived from *GOES-7* 11-μm radiances using the Barnes interpolated temperature and humidity profiles, as discussed previously, and a transmittance model (McMillin and Fleming 1976) to account for the atmospheric attenuation. An 11-μm surface emissivity of 0.98 was assumed in these calculations. The potential sources of uncertainty in the skin temperature estimations include uncertainties in the transmittance model and humidity–temperature profiles, and the use of a constant IR surface emissivity.

As seen in Fig. 2, when the IR-derived skin temperatures are included, the predicted values are in better agreement with the observations, particularly for the ascending passes. The rms errors are reduced in all cases where the linear correlations are about 0.92 and 0.83 for the ascending and descending passes, respectively. This clearly demonstrates that the biases observed in Fig. 1 are due mainly to incorrect specification of the skin temperature. The results of Fig. 2 also suggest that the scatter in these relationships is most likely caused by variations in the microwave surface emissivities, although satellite navigation errors and instrument noise also presumably contribute to the scatter.

One other characteristic of Fig. 2 is that the horizontal

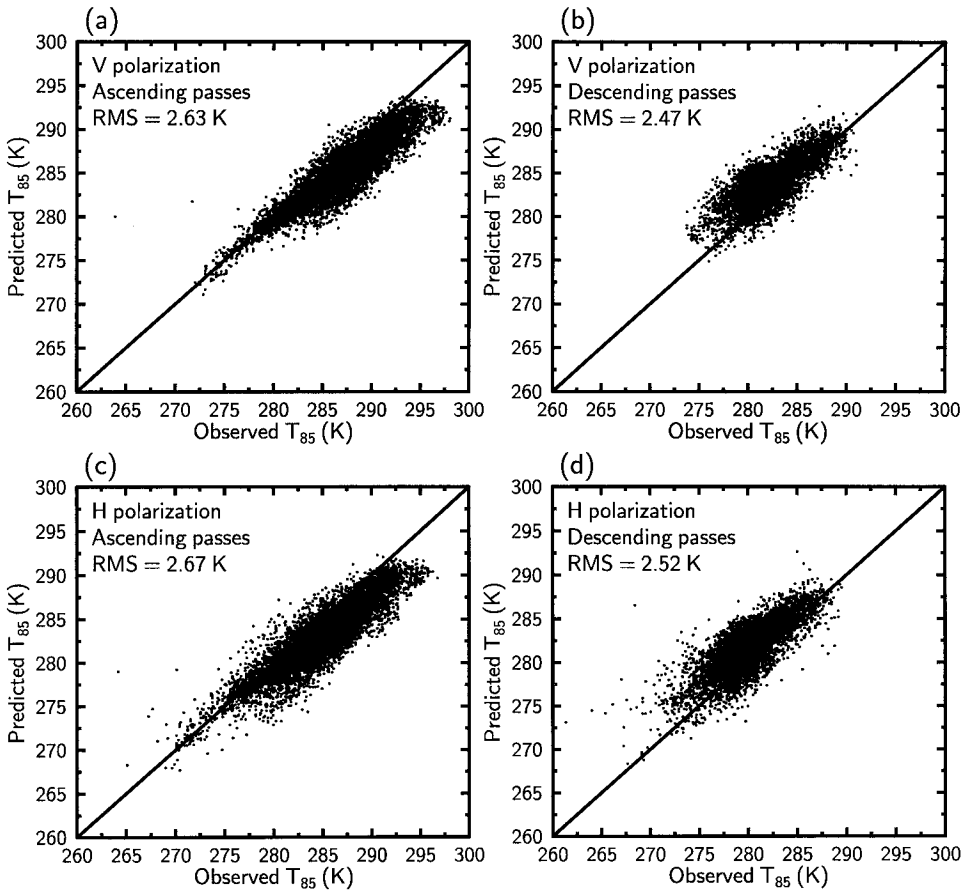

FIG. 1. Scatter diagrams of predicted 85.5-GHz brightness temperatures at (top) vertical and (bottom) horizontal polarization versus SSM/I observed brightness temperatures over land for clear sky, divided into ascending (0900–1000 local time) (left) and descending (2000–2100 local time) (right) DMSP overpasses. Surface air temperatures were used to approximate the skin temperature in the simulations. Lines of perfect agreement and the root-mean-square errors are also indicated.

polarization results have slightly greater scatter (as seen in the rms errors) than the vertical polarization results. This is due to the horizontal component being more sensitive to surface moisture than the vertical component, which might be caused by recent rainfall events or local irrigation. Despite the slightly greater noise at this polarization, this problem can be usually overcome in the cloud liquid water retrievals since the brightness temperature at horizontal polarization is more sensitive to cloud liquid water than at vertical polarization due to its lower surface emissivity.

In summary, these comparisons confirm that the surface emissivities over 7 days, at least for this region and season, are very stable. Thus the composites provide a useful background for which to retrieve cloud liquid water. Also, accurate knowledge of the skin temperature is a crucial element in correctly simulating clear-sky SSM/I brightness temperatures over land. This may have direct implications for cloud liquid water retrievals since an incorrect skin temperature might lead to large biases in the retrievals. However, under cloudy conditions one might expect the surface air temperature and the skin temperature to usually be similar. In addition, these results also show that in order to detect cloud liquid water at 85.5 GHz over land surfaces one must be above the clear-sky noise level of approximately 2.5 K.

4. Microwave detection of cloud liquid water over land

Within this section observations are used to provide a simple demonstration of the capability of passive microwave radiometry to sense cloud liquid water (CLW) over land surfaces at 85.5 GHz. The High Plains region of the northern United States was selected for this demonstration. This region is desirable since there are relatively few small lakes to affect the surface emissivity and the surface temperatures are relatively uniform across the region.

GOES-7 imagery of the visible and infrared (11 μm) channels at 1530 UTC 9 August 1991 for eastern Montana and North Dakota is shown in Fig. 3. This specific

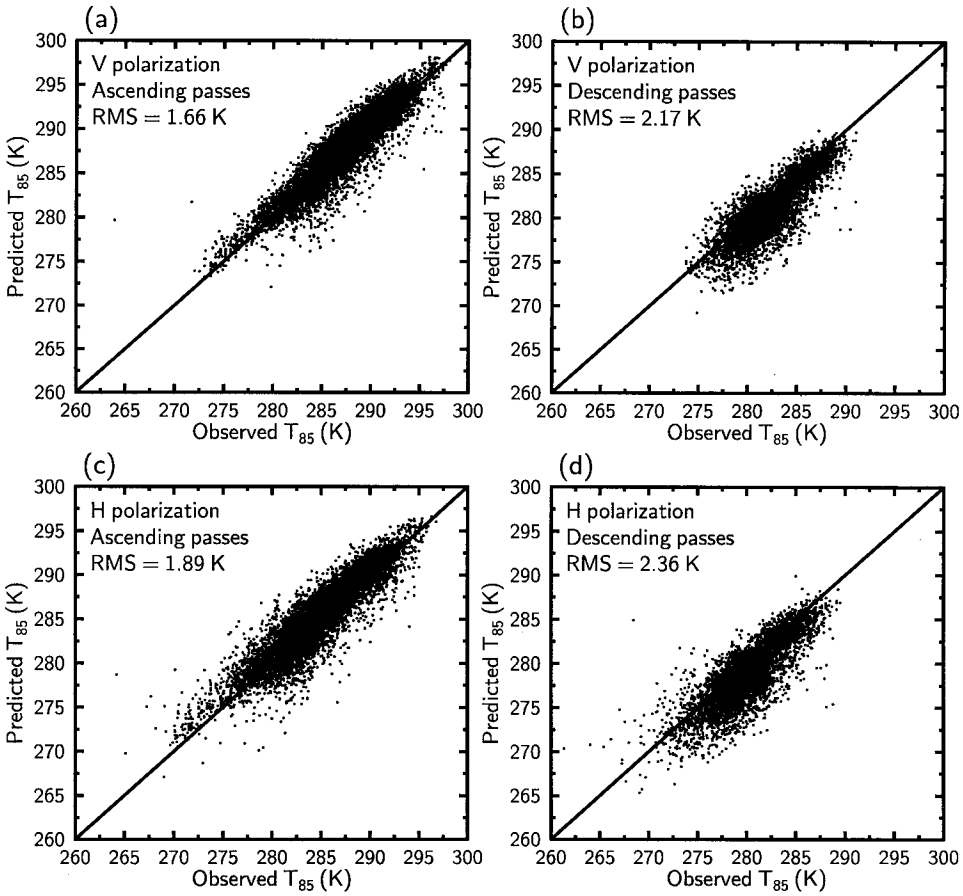

FIG. 2. Same as in Fig. 1 but using skin temperatures derived from *GOES-7* IR measurements in the simulations.

image was chosen because it contains a variety of cloud types. The main feature of interest is the elongated cloud system oriented north to south in eastern Montana. Another cloud feature is an extensive deck of low-level clouds in south-central North Dakota.

Observations from the 85.5-GHz vertical polarization channel of the SSM/I at 1540 UTC for the same day are given in Fig. 4a. The horizontal polarization observations are not shown since the results are similar. Significant brightness temperature depressions are evident (T_b's as low as 243 K) for the cloud system in eastern Montana, particularly near the Canadian border, which is a probable indication of precipitation. Also, several lakes clearly stand out in this image as cold regions, including Lake Sakakawea in west-central North Dakota and Fort Peck Lake in eastern Montana, due to the much lower emissivity of water surfaces.

One way to illustrate the detection of CLW at 85.5 GHz is to subtract the emission at the surface (i.e., the emission in the absence of an atmosphere) from the instantaneous SSM/I observations. This difference can be thought of as a measure of the absorption resulting from gaseous absorption (primarily H_2O) and cloud liquid water droplets (absorption by cloud ice particles is negligible at microwave frequencies). For precipitating clouds, however, this difference is more difficult to interpret since scattering processes also contribute to the brightness temperatures measured at the TOA.

A companion distribution of the emission at the surface at 85.5-GHz vertical polarization is depicted in Fig. 4b. This quantity was estimated by simply multiplying the surface emissivity by the surface skin temperature. The surface emissivities are a composite for the period 7–14 August 1991. Interpolated surface air temperatures (as done for the clear-sky analysis) were used to approximate the skin temperature. The identifying marks of lakes and rivers are more prominent in the surface emission field, as expected. These features are also somewhat broader in appearance than in Fig. 4a, due mainly to uncertainties in the SSM/I's geolocation when creating the surface emissivity composites.

The resultant difference field is shown in Fig. 5. Large, positive values of the absorption (up to 21 K) exist over lakes and rivers. This apparent ''enhanced absorption'' can be explained as a larger contribution from the surface reflected atmospheric term in (1) for a low-emissivity background. A large region of significant negative values (typically about -4 to -6 K, but

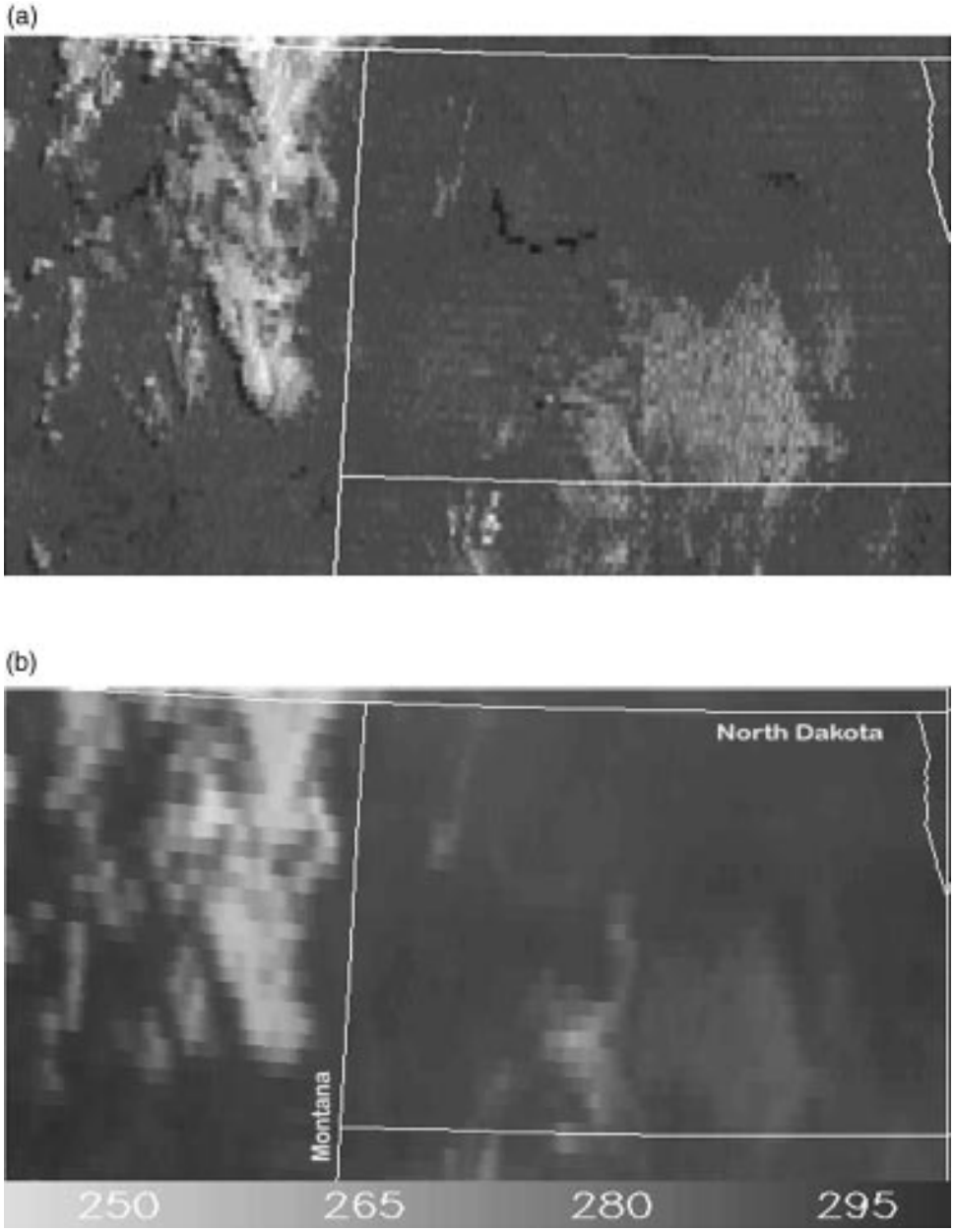

FIG. 3. *GOES-7* reduced resolution (a) visible and (b) infrared (11 μm) images over North Dakota and eastern Montana for 1530 UTC 9 August 1991. Infrared brightness temperatures are in kelvins.

can be as great as -45 K) corresponds precisely to the location of the cloud system in eastern Montana (cf. Fig. 3). This cloud signature emerges due to the additional absorption by CLW. The values are negative because a depression of the brightness temperature at 85.5 GHz generally occurs when clouds are present over high emissivity surfaces, such as land (e.g., Spencer et al. 1989). Note that other cloud features, such as the low clouds in south central North Dakota, remain undetected. This phenomenon will be discussed in more detail in the next section.

To ensure that the cloud signal observed in Fig. 5 is primarily the result of absorption by cloud droplets and not scattering by precipitation-sized particles, the scattering index of Grody (1991) was used to screen for precipitating clouds. These areas are colored black and marked with a ''P'' in Fig. 5. As anticipated, extensive areas in the northernmost part of the cloud system contain precipitating clouds, while much of the rest of the cloud system is nonprecipitating.

A more quantitative comparison can be done by examining the profiles of various quantities through different parts of the cloud system. The locations of two such profiles are shown in Fig. 5—one along the same

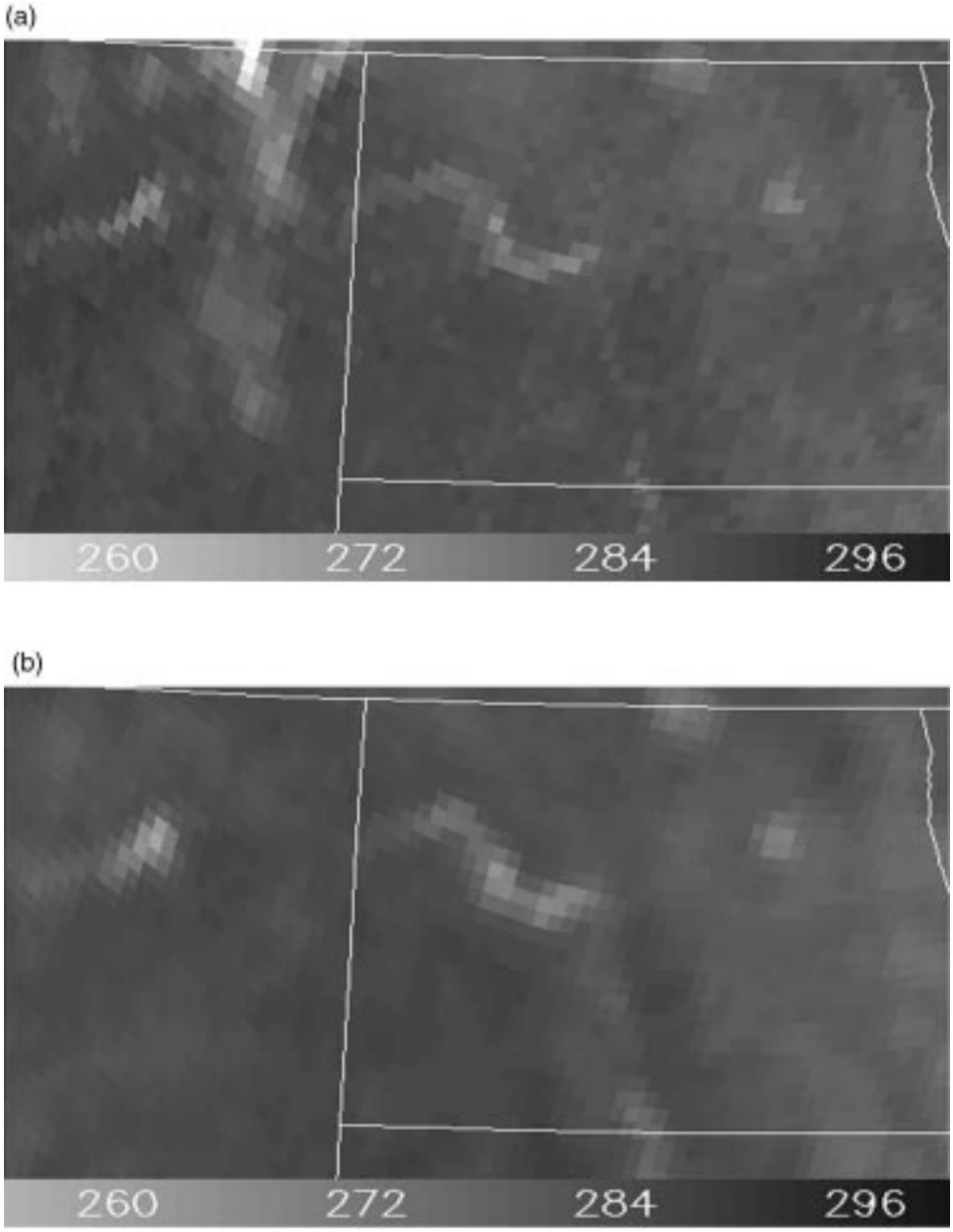

FIG. 4. Same as Fig. 3 except (a) SSM/I brightness temperatures (K) for 85.5-GHz vertical polarization and (b) estimate of microwave surface emission at vertical polarization (K) based on a 7-day surface emissivity composite and interpolated surface air temperatures.

element of sequential SSM/I scans (A) and one along a single SSM/I scan line (B). The results for profiles A and B are presented in Fig. 6 and 7, respectively, and include the visible counts and IR brightness temperatures from *GOES-7,* the 85.5-GHz vertical polarization observations from the SSM/I in Fig. 4a, and the microwave surface emission from Fig. 4b. SSM/I FOVs tagged as containing probable precipitation, determined by the Grody (1991) method, are also indicated.

In Fig. 6 one can see for profile A (left to right in the figure roughly corresponds to north to south) that the differences between the surface emission and the SSM/I brightness temperatures are typically about 5–8 K, but can exceed 10 K. Also, notice how the SSM/I T_b's closely follow the independent signatures of the cloud given by the visible and IR measurements, even outside of precipitating regions. This is clear and dramatic proof of the ability of the SSM/I's 85.5-GHz channels to sense CLW over land. In clear regions (i.e., scan line numbers greater than about 45) the SSM/I brightness temperatures are generally slightly higher ($\approx$2–4 K) than the surface emission, which is caused by a slight

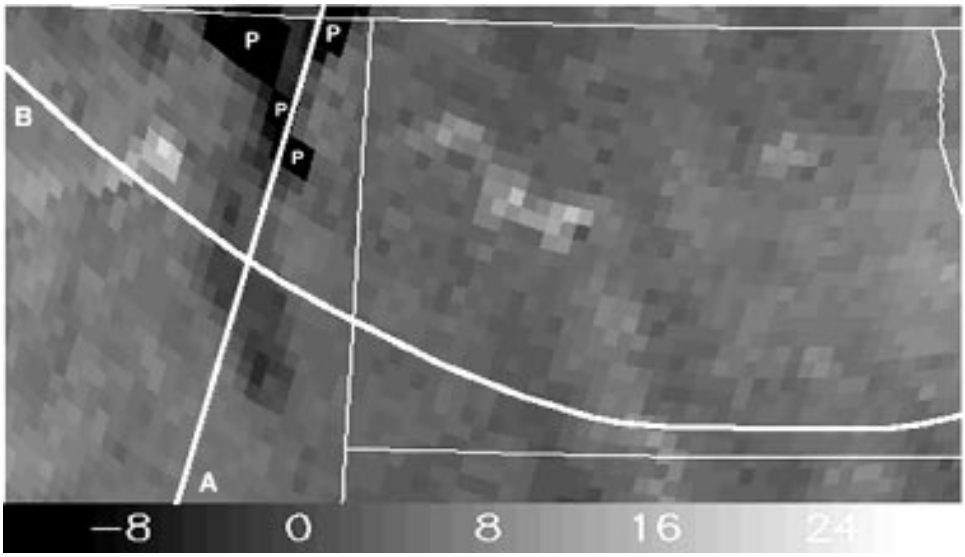

FIG. 5. SSM/I 85.5-GHz brightness temperature at vertical polarization minus the surface emission (K). The absolute difference provides a measure of the absorption due to the atmosphere and clouds. Areas identified as containing precipitating clouds, as determined from the Grody (1991) scattering index method, are black and marked with a ''P.'' Also shown are the location of the profiles through the same SSM/I element number of sequential scans (A) and along a SSM/I scan line (B).

brightening (1–2 K) by water vapor absorption/emission and by an underestimation of the skin temperature in the calculation of the surface emission, as seen in Fig. 1 for the ascending passes.

For profile B in Fig. 7, a number of different and more complex characteristics can be seen. In this figure left to right is defined as roughly west to east. There is an 85.5-GHz brightness temperature depression for the southern parts of the cloud system as well, which is located near element 85, but the depression is much less than that seen in Fig. 6, being just under 5 K. Recall that it is the difference between the observed brightness temperature and the *clear-sky* brightness temperature that determines the strength of the CLW signal. Hence, the clear-sky T_b is likely about 2 K higher than the surface emission, thus providing an actual CLW signal of about 5–6 K. Even a small signal such as this is still above the clear-sky noise level of about 2.5 K (from

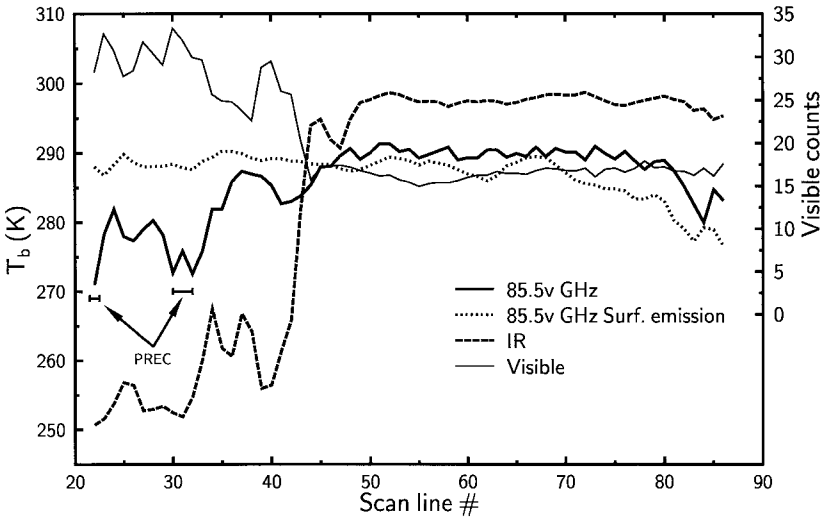

FIG. 6. Profile A through the cloud system consisting of the SSM/I 85.5-GHz vertical (V) polarization brightness temperatures (K), the surface emission at 85.5V GHz (K), the IR brightness temperatures (K), and visible counts from *GOES-7* as a function of scan line number. SSM/I pixels determined to contain precipitation based on the Grody (1991) method are also indicated.

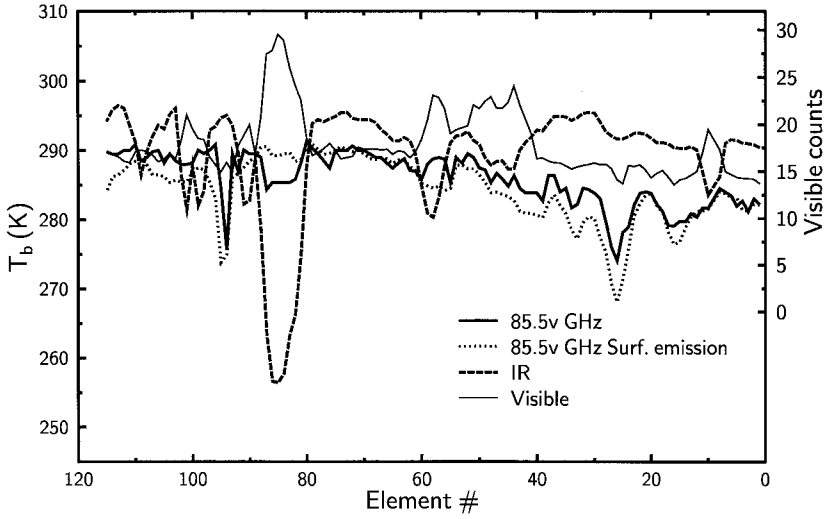

FIG. 7. Same as Fig. 6 but for profile B and as a function of element number.

section 3), and thus a retrieval of cloud LWP is possible. Two major dips that occur in the SSM/I observations and the surface emission are lakes. The depression near element 95 is caused by Fort Peck Lake in Montana, and that near element 25 is caused by Lake Oahe in North Dakota.

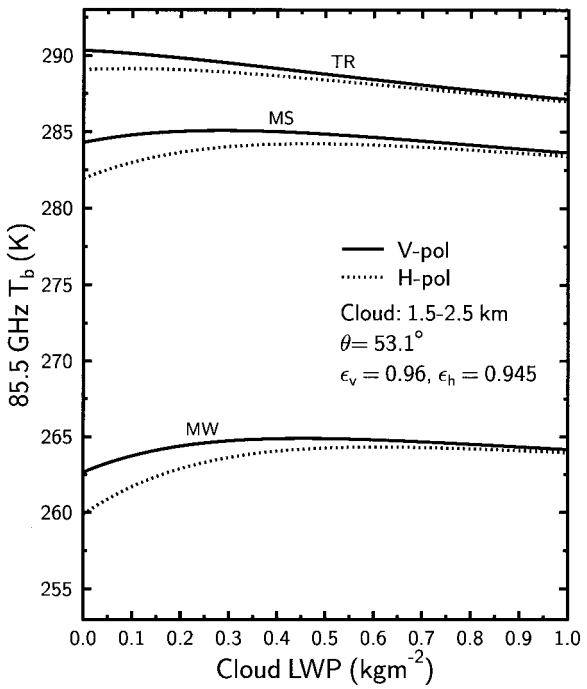

FIG. 8. Theoretical calculations of 85.5-GHz brightness temperatures (K) at vertical and horizontal polarization versus cloud liquid water path for a low-lying cloud (1.5–2.5 km) over a land surface. The calculations were done at a zenith angle θ of 53.1° and for three different sets of temperature–humidity profiles taken from McClatchey et al. (1972): tropical (TR), where the integrated water vapor is 42 kg m^{-2}; midlatitude summer (MS), where PWC = 20 kg m^{-2}; and midlatitude winter (MW), where PWC = 8.8 kg m^{-2}.

As discussed previously, the low clouds detected at the visible wavelengths for elements 40–60 are virtually unseen by the SSM/I. However, there appears to be evidence of a small brightening effect in the microwave brightness temperatures for the slightly higher cloud located near element 60. As will be shown in the following section, under certain circumstances, clouds over land surfaces can cause a brightening at 85.5 GHz.

5. Overview of limitations of microwave retrievals

While it has been demonstrated that passive microwave measurements of moderately high frequency are useful for detecting CLW over land, there are numerous difficulties in the problem of retrieving the cloud LWP. In this section, a brief description of these limitations is provided with the help of theoretical calculations.

Calculations were done based on (1) for different atmospheric conditions as a function of LWP for strictly nonprecipitating clouds. Surface emissivities of ϵ_V = 0.96 and ϵ_H = 0.945 were assumed using typical observed values from the clear-sky analysis. The tropical, midlatitude summer, and midlatitude winter humidity and temperature profiles from McClatchey et al. (1972) were also used. The humidity profile for the midlatitude summer was adjusted slightly to give an integrated water vapor amount of 20 kg m^{-2}. The atmospheric attenuation was computed from the Liebe et al. (1993) MPM.

Figure 8 shows the results of calculations for 85.5 GHz at a zenith angle of 53.1° for a 1-km-thick cloud situated from 1.5 to 2.5 km, where the ground level is at 1 m. For this type of cloud the response at 85.5 GHz to cloud liquid water is very small. Indeed, this lack of sensitivity has significant implications for retrieval methods that use a single SSM/I channel to estimate LWP for low clouds. This behavior explains the inability of measurements at vertical polarization (or horizontal

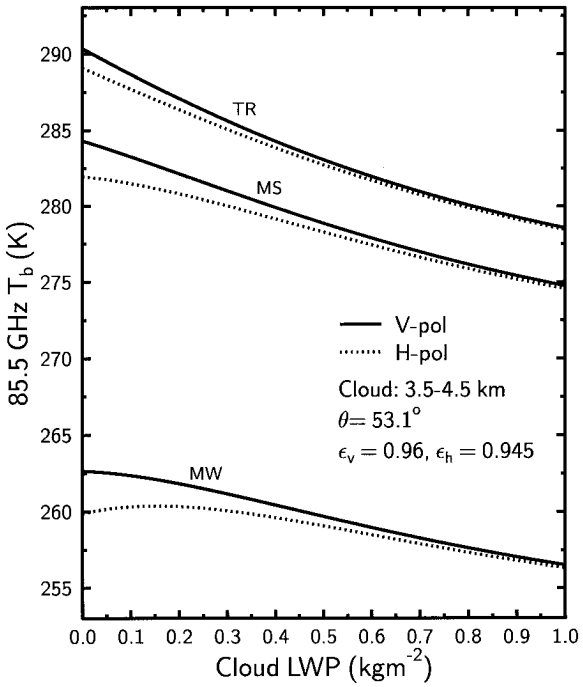

FIG. 9. Same as Fig. 6 except for a midlevel cloud (3.5–4.5 km).

polarization) to sense the low cloud deck, as shown in Fig. 5. These results are also consistent with the conclusions of JV90, who found that errors in their cloud LWP retrievals were greatest for the lowest-level clouds in their analysis.

Another interesting result is that a brightening effect at 85.5 GHz, although small, can occur for clouds over land, as seen for the midlatitude winter and summer atmospheres. [Spencer et al. (1989) also showed a brightening effect for low clouds over land, but under different surface and atmospheric conditions.] Note, however, that the results in Fig. 8 are based on a single set of surface emissivities—whether or not a brightening or depression occurs in the brightness temperatures depends critically on the magnitude of the surface emissivity components.

When the same cloud is moved to a greater height (3.5–4.5 km), as shown in Fig. 9, a depression results in the brightness temperatures relative to the clear sky for almost all atmospheres and both polarizations. This behavior is a result of the effective emission height of the atmosphere moving to increasingly higher levels in the atmosphere, where the emission occurs at colder temperatures. The results for the midlatitude summer profiles are also quantitatively consistent with the SSM/I observations in cloudy regions, as shown, for example, in Fig. 6.

The retrieval method developed by JV90 is a physically based approach that finds an iterative solution to either the vertical or horizontal polarization equations in (1). This method will be referred to as the single-channel (SC) method throughout the remainder of this paper. Briefly, their method makes use of surface emissivity composites derived from microwave and IR measurements in clear-sky regions and uses data from nearby radiosondes to characterize the vertical temperature and humidity structure of the atmosphere. The sounding profiles are used, along with a microwave absorption model (e.g., Liebe et al. 1993), to compute the atmospheric attenuation. These profiles are also used to estimate the cloud-base pressure and, along with IR measurements, the cloud-top pressure. Once this information is determined, all that remains is to add cloud liquid water to the cloud layer(s) until the brightness temperature computed from (1) matches the observed brightness temperature within a desired precision. This method is only valid for nonprecipitating clouds since (1) assumes a purely absorbing–emitting atmosphere.

One of the major weaknesses of the SC method and even the new method introduced in this paper is their reliance on surface observations and radiosonde measurements. Not only are these retrieval methods not applicable in regions that lack these types of ancillary measurements, but time differences between the satellite overpass and the launch time of the radiosonde (0000 or 1200 UTC) can lead to additional uncertainties in the retrievals.

Errors in the cloud LWP retrievals originate from a variety of different sources. These include uncertainties in the MPM, the vertical distribution of liquid water, and the cloud-base and cloud-top heights, among others. Diak (1995) found that multilevel clouds can introduce further errors in microwave retrievals. In evaluating the errors in the SC method, JV90 also determined that the method was sensitive to the assumed freezing level of the cloud. While important, a detailed error analysis of the retrieval methods discussed here is, unfortunately, beyond the aim of this study and will be addressed in a future study.

Other potential difficulties that can generally plague microwave retrievals involve variations in surface emissivity and broken cloudiness. Increases in surface moisture from irrigation and, particularly, rainfall events in certain regions can often reduce the surface emissivity to such an extent that it is significantly smaller than the 7-day composite emissivity. In these cases the retrieval will likely greatly overestimate the cloud LWP. Therefore, care must be taken in identifying these situations. One example of the effect of a rainfall event on the retrievals is described in section 7.

The problem of retrieving cloud liquid water under broken cloudiness is important since microwave measurements from space are typically of coarse spatial resolution. The study of JV90 addressed this issue and found that the retrieval errors were greatest for the smallest cloud LWP and sparse cloudiness. However, these effects may be at least partially accounted for by using IR and/or visible data to help in quantifying the degree of cloudiness within the FOV of the SSM/I.

6. Normalized polarization difference method

To overcome some of the potential deficiencies in the SC method a new method is introduced that makes use of the polarization difference of the brightness temperatures. Such an approach is appealing because it has a simple physical basis—that is, the intervening atmosphere and clouds, through absorption and emission processes, act to depolarize the radiation emitted by a polarized surface. Because water surfaces are highly polarized, this type of method has also been exploited over the oceans in the measurement of integrated water vapor (Tjemkes et al. 1991) and cloud liquid water (Petty 1990).

Using (1), the difference between the V-polarization and H-polarization intensities can be expressed as

$$I_V - I_H = (\epsilon_V - \epsilon_H)B(T_s)\tau - (\epsilon_V - \epsilon_H)\tau^2 \int_{p_s}^{0} \frac{B[T(p)]}{[\tau(p, 0)]^2}\frac{\partial\tau(p, 0)}{\partial p}\,dp - (\epsilon_V - \epsilon_H)\tau^2 B(T_{cos}), \quad (2)$$

where the frequency dependence has been dropped for clarity. An important consequence of this operation is that one of the atmospheric integral terms cancels. Another simplification can be made by applying the Rayleigh–Jeans law to the intensities I_V and I_H in (2) to yield the following for the polarization difference of the brightness temperatures:

$$\Delta T_b \approx \frac{c^2}{2Kv^2}\Delta\epsilon\tau\left\{B(T_s) - \tau\int_{p_s}^{0} \frac{B[T(p)]}{[\tau(p, 0)]^2}\frac{\partial\tau(p, 0)}{\partial p}\,dp - \tau B(T_{cos})\right\}, \quad (3)$$

where $\Delta\epsilon = \epsilon_V - \epsilon_H$, c is the speed of light and K is Boltzmann's constant.

A disadvantage of using the Rayleigh–Jeans law as opposed to the Planck function is that it can introduce errors in ΔT_b. However, these errors are expected to be small since the Planck function is nearly linear at all SSM/I frequencies. For the anticipated range of water vapor and cloud liquid water the errors arising from this approximation at 85.5 GHz are found, based on theoretical calculations, to be less than 0.01 K. When applying (3) in the retrieval we use instead the quantity $\Delta T_b/\Delta\epsilon$, which gives the method its name: the *normalized* polarization difference (NPD) method. The general procedure for retrieving cloud LWP is identical to that of the SC method.

To gain further insight into how ΔT_b behaves at 85.5 and 37 GHz over land surfaces we turn to model calculations. The frequency of 37 GHz was also chosen since it is the SSM/I frequency that is second most sensitive to cloud liquid water. In Fig. 10, theoretical calculations of ΔT_b versus cloud LWP are presented for the same clouds, surface emissivities, and atmospheric conditions as in Figs. 8 and 9. As expected, the polarization difference decreases as a function of cloud LWP at both frequencies. The polarization difference at 37 GHz is always greater than at 85 GHz since there is less water vapor and liquid water absorption at this frequency. The response to cloud LWP, while highly nonlinear at 85.5 GHz, is nearly linear at 37 GHz. In addition, the ΔT_b signal at 85 GHz for the tropical atmosphere is less than half that for the midlatitude winter atmosphere, which is caused by the depolarization effects of the additional water vapor. In contrast, at 37 GHz, ΔT_b is far less dependent on the amount of water vapor since the attenuation by the water vapor continuum at this window frequency is much weaker than at 85 GHz.

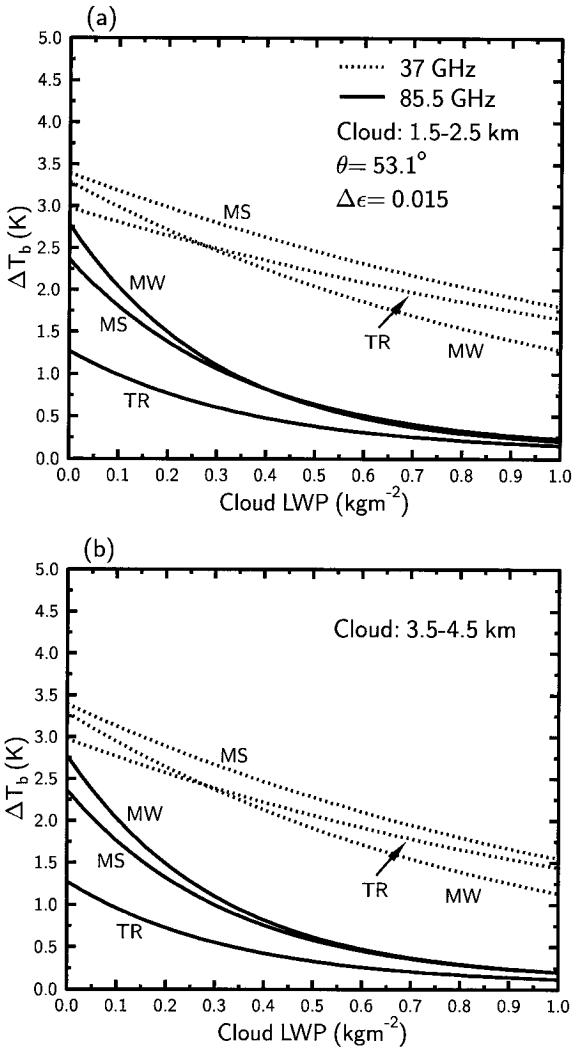

FIG. 10. Theoretical calculations of the polarization difference (ΔT_b) at 85.5 and 37 GHz as a function of cloud LWP for a 1-km-thick (a) low cloud and (b) midlevel cloud for the same three atmospheres as described in Fig. 8.

The varied responses of these frequencies under different atmospheric and cloud conditions have several important ramifications for retrieving cloud liquid water over land surfaces. First, for clouds with high amounts of LWP (greater than 0.5 kg m^{-2} or so) it is clear that the polarization difference will be less useful at 85.5 GHz since the sensitivity of ΔT_b to cloud LWP is greatly reduced. However, this is true for the value of $\Delta\epsilon$ specified in the calculations; more polarized land surfaces might make the 85.5-GHz frequency more useful at larger cloud LWP. At 37 GHz the sensitivity is higher for larger cloud LWP and suggests this frequency could be used for retrievals in nonprecipitating clouds with high LWP. The results also show that in atmospheres with an abundance of water vapor, such as in the Tropics, the ability to measure cloud LWP at 85.5 GHz is significantly reduced, but retrievals at 37 GHz might be possible since the magnitude of ΔT_b remains large.

There are many important advantages to the polarization difference approach. For example, the SC method, as discussed previously, suffers from an inability to detect low clouds, no matter how much liquid water is contained in the cloud. But from Fig. 10a we can see that low clouds become detectable from a polarization difference perspective.

One of the most important advantages this method has over the SC method is that ΔT_b is extremely insensitive to changes in the surface skin temperature; hence, precise knowledge of the skin temperature is less crucial in the retrievals. This can be demonstrated by taking the partial derivative of (3) with respect to T_s, which gives

$$\frac{\partial \Delta T_b}{\partial T_s} \approx \Delta\epsilon\tau\left(\frac{h\nu}{KT_s}\right)^2 \frac{e^{h\nu/KT_s}}{(e^{h\nu/KT_s} - 1)^2},$$

where h is Planck's constant and $\partial\Delta\epsilon/\partial T_s$ is ignored since it is negligible. At 85.5 GHz, and using $T_s = 294$ K, $\Delta\epsilon = 0.02$, and a typical cloudy atmospheric transmittance of 0.58, it follows that $\partial\Delta T_{85}/\partial T_s \approx 0.011$. This means that a 1-K perturbation in T_s results in a very small change of 0.011 K in ΔT_{85}. At 37 GHz (using $\tau = 0.82$) the sensitivity is 0.016, which is slightly larger since the atmosphere is more transparent at this frequency. The high insensitivity of ΔT_b to changes in T_s results primarily from the small values of $\Delta\epsilon$ that occur over land and the extremely low sensitivity of $\Delta\epsilon$ to changes in T_s.

Yet another advantage is that the polarization difference becomes dependent on the relative accuracy of the measurements rather than their absolute accuracy. Therefore, even though the magnitude of the polarization difference at 85.5 GHz in cloudy regions can often be less than 2 K, which is about the estimated absolute accuracy of the individual SSM/I measurements (Hollinger et al. 1990), the polarization difference is affected by *interchannel* relative accuracies that are, based on preflight calibration, within 0.2 K over a broad range of temperatures (Hollinger et al. 1987).

The major disadvantage of this approach is that in principle it can only be applied when the surface is polarized (i.e., $\Delta\epsilon > 0$). However, this is not as severe a limitation as it first appears since the results from Jones (1996) indicate that a small surface polarization signal is measurable and very common over many land regions, with the notable exception of forested regions. Figure 11 shows frequency histograms of observed values of 85.5-GHz $\Delta\epsilon$ for four selected regions over the United States, including the Southeast (31°–36°N, 83°–93°W), Midwest (37°–41°N, 83°–93°W), central Great Plains (37°–43°N, 95°–105°W), and southern Great Plains (31°–37°N, 95°–105°W). These results are constructed from a 69-day composite for 28 July 1991 to 4 October 1991. Note that permanent features such as lakes and rivers have not been excluded and will contribute to larger polarization differences.

Regional differences in the frequency distributions of $\Delta\epsilon$ are evident in Fig. 11. For the southeast region, the distribution of $\Delta\epsilon$ is somewhat broader than elsewhere and the values are generally lower (mode value of 0.0055). Also, this region has the largest percentage of nonpolarized surfaces as compared to the other regions. This behavior is likely the result of the greater abundance of vegetation, which generally has a depolarizing effect at microwave frequencies. A greater occurrence of higher polarized surfaces is seen for both Great Plains regions (Figs. 11c,d), where the mean and mode of $\Delta\epsilon$ is the highest.

As further evidence to show that the polarization signature over many land surfaces is real and that the NPD retrieval method is viable, we show in Fig. 12 the predicted versus observed ΔT_b at 85.5 GHz (ΔT_{85}) for the same clear-sky observations used in Fig. 2. Data from both ascending and descending DMSP overpasses are included. If a surface polarization difference signal were not detectable over these land surfaces, then little, if any, correlation would exist between the predicted T_b's and the observations. Yet what we find from Fig. 12 is that there is in fact a reasonably strong correlation between the predicted and observed values. A least squares linear fit yields a correlation of 0.716, which is statistically significant at the 99% confidence level. There also appears to be a small bias for the smallest values of ΔT_{85}, where the predicted values have a residual of about 1 K when the observations are nonpolarized. This bias may be an artifact of the 7-day surface emissivity composites.

The scatter in Fig. 12, as represented by the rms error of 1.03 K, is attributed principally to variations in surface emissivity as a result of using 7-day composites. This figure also illustrates that it is not possible to retrieve cloud LWP for *clear-sky* values of ΔT_{85} below roughly 1 K since the cloud signal is essentially buried in the noise. This has relevance to the theoretical results in Fig. 10 because it indicates that the NPD method at

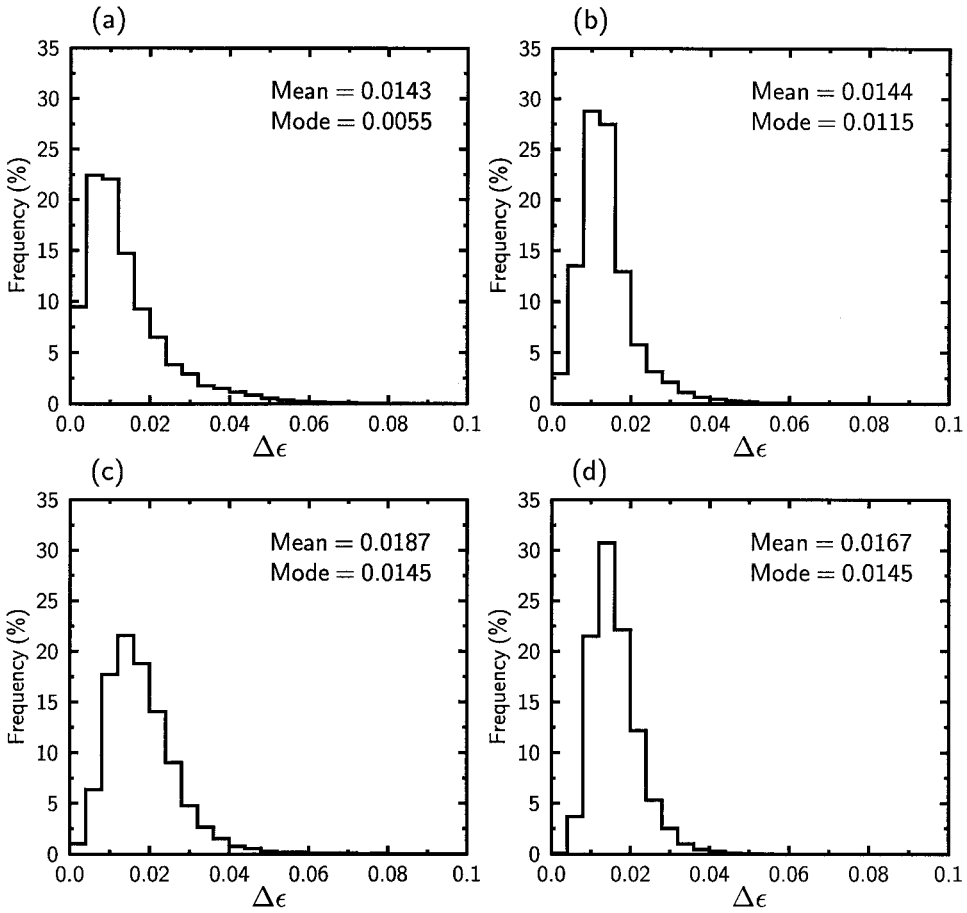

FIG. 11. Frequency histograms of observed surface emissivity polarization differences $\Delta\epsilon$ at 85.5 GHz over the United States for the (a) Southeast (31°–36°N, 83°–93°W), (b) Midwest (37°–41°N, 83°–93°W), (c) central Great Plains (37°–43°N, 95°–105°W), and (d) southern Great Plains (31°–37°N, 95°–105°W). Also indicated are the mean and the mode for each distribution.

85.5 GHz is inapplicable for a tropical atmosphere when $\Delta\epsilon = 0.015$. However, if surface emissivity composites were available over a shorter time period, such as 1 or 2 days, then the noise level might be reduced enough to make a retrieval possible; but when using 7-day composites of surface emissivity there is a better chance of retrieving cloud LWP for larger clear-sky values of ΔT_{85} where there exists a larger cloud signal relative to the noise level.

7. Intercomparison of normalized polarization difference and single-channel methods

In our comparison of the NPD method and the SC method we use ground-based microwave radiometer observations of LWP. The comparison with ground observations is not intended to serve as a retrieval validation, but rather as an independent test to evaluate the relative strengths and weaknesses of the different methods since the ground observations are considered more accurate than the satellite-based observations. The region of the intercomparison is near Platteville, where the ground radiometer is located. A total of 22 cases were compiled for August and September of 1991. In applying the SC and NPD methods we used observations of the air temperature from surface stations (at the hour closest to the satellite overpass), radiosonde profiles from Denver, and the Liebe et al. (1993) MPM.

a. Clear-sky cases

Estimating cloud liquid water in cloud-free areas can yield a quantitative measure of the minimum uncertainties in the retrievals. This is frequently done for microwave retrievals over oceanic regions (e.g., Petty 1990; Greenwald et al. 1993). While this is not always possible with the physical methods described in this study, retrievals were done for several of the 13 clear-sky cases, and the results are summarized in Table 2. An average of the four retrievals closest to the Platteville site was used. Those cases in which a retrieval is not given were generally the result of the cloud-top pressure being

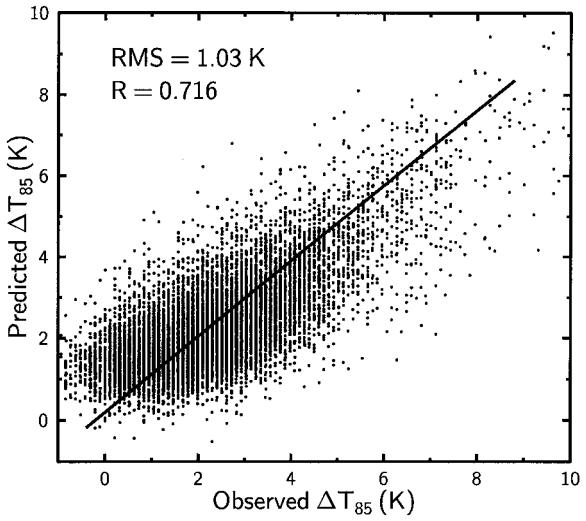

FIG. 12. Scatter diagram of predicted 85.5-GHz polarization difference (ΔT_{85}) versus SSM/I-observed ΔT_{85} for the same clear-sky data used in Fig. 2. Data for both ascending and descending passes are included. The root-mean-square (rms) error and the line and correlation coefficient R determined from a least squares fit are also shown.

greater than the cloud-base pressure derived from the sounding. The integrated water vapor (PWC) and LWP observations derived from the ground radiometer are given as a ± 0.5-h average from the satellite overpass time. As seen in Table 2, there are occasional high biases in the ground observations of LWP (e.g., case 5), but clear sky conditions are always characterized by very low standard deviations of less than 0.01 kg m^{-2}. Also indicated are the average observed polarization differences of the brightness temperatures at 85.5 GHz and the composite surface emissivities for the four nearest pixels. Note in Table 2 that the surface polarization differences around the Platteville site are slightly higher than average when compared to the regional frequency histogram in Fig. 9c. This may be caused by the extensive irrigation in this region (see, e.g., JV90).

Excluding case 18, which is a special case, it is found that the two SC method retrievals are widely varying, where the overall average uncertainty is about 0.12 kg m^{-2}. We should emphasize that this value is probably not representative of the true minimum errors since the sample is very small. On the other hand, the retrievals for the NPD method are much less variable and lower, where the average uncertainty is about 0.08 kg m^{-2}.

One case of particular interest is case 18. Here, approximately 0.9 in. of rain had fallen over Platteville, according to a nearby surface station, about 3–4 h prior to the DMSP overpass. This is a severe test for the retrieval methods since the emissivity composite may not be representative of the surface conditions at the time of the satellite overpass. As shown in Table 2 the SC retrievals for case 18 are the largest of all the cases. These retrievals are useful in that they provide an indication of the magnitude of the errors that can occur in these situations. In contrast, the NPD method is, relatively speaking, much less affected by changes in the surface emissivity, although the retrieval is slightly higher than for the other cases. The likely reason is that although the surface moisture reduces the emissivity for both polarizations, the polarization *difference* $\Delta\epsilon$ is impacted to a lesser degree.

b. *Cloudy-sky cases*

The remaining nine cases were classified as being cloudy, with one case being excluded (case 3), since

TABLE 2. Results of the single-channel (SC) and normalized polarization difference (NPD) retrievals (kg m^{-2}) for the clear-sky cases over Platteville, Colorado. Integrated water vapor (PWC) and the liquid water path (LWP), as determined from the ground (Grd) microwave radiometer, are also included and consist of a 1-h average centered on the satellite overpass time and the standard deviation. The average polarization difference at 85.5 GHz from the SSM/I and the average surface polarization difference at 85 GHz ($\Delta\epsilon$) from the composite are also shown.

Case No.	Grd PWC (kg m^{-2})	Grd LWP (kg m^{-2})	NPD method (kg m^{-2})	SC method V-pol (kg m^{-2})	SC method H-pol (kg m^{-2})	SSM/I ΔT_{85} (K)	$\Delta\epsilon$
1	21.7	−0.001 ± 0.0017	—	—	—	2.72	0.026
2	23.7	0.019 ± 0.0017	0.089	0.245	0.189	2.62	0.025
5	26.2	0.043 ± 0.0020	—	—	—	2.79	0.026
6	17.3	0.007 ± 0.0021	—	—	—	3.32	0.024
7	17.9	−0.0017 ± 0.0039	*0.062	*0.336	—	4.58	0.024
10	22.7	0.034 ± 0.0023	0.091	0.017	0.041	2.98	0.022
12	22.5	0.020 ± 0.0011	*0.074	*0.013	0.025	2.20	0.021
13	19.6	0.0097 ± 0.0032	—	—	—	2.28	0.020
15	18.3	0.0029 ± 0.0027	—	—	—	4.26	0.024
17	19.7	0.034 ± 0.0079	—	—	—	2.85	0.025
18	21.7	0.013 ± 0.0058	0.138	0.518	0.764	2.70	0.024
19	17.8	0.017 ± 0.0062	—	—	—	2.62	0.023
21	18.2	0.025 ± 0.0062	—	—	—	2.85	0.027

* One data point used in average.
H-pol—horizontal polarization.
V-pol—vertical polarization.

TABLE 3. Same as Table 2 except for cloudy-sky retrievals, which also include the standard deviations of the retrievals.

Case No.	Grd PWC (kg m^{-2})	Grd LWP (kg m^{-2})	NPD method (kg m^{-2})	SC method V-pol (kg m^{-2})	SC method H-pol (kg m^{-2})	SSM/I ΔT_{85} (K)	$\Delta\epsilon$
4	27.7	0.114 ± 0.037	0.136 ± 0.066	0.105 ± 0.076	0.099 ± 0.065	2.54	0.028
8	23.0	0.224 ± 0.039	0.357 ± 0.143	—	—	0.92	0.022
9	24.7	0.121 ± 0.017	0.206 ± 0.137	0.156 ± 0.028	0.044 ± 0.003	1.86	0.023
11	22.7	0.079 ± 0.074	0.043 ± 0.012	0.044 ± 0.021	0.030 ± 0.016	3.20	0.021
14	23.6	0.047 ± 0.040	0.058 ± 0.070	*0.063	*0.004	1.88	0.020
16	22.1	0.030 ± 0.013	0.133 ± 0.120	0.318 ± 0.097	0.373 ± 0.261	2.70	0.023
20	26.3	0.079 ± 0.021	0.148 ± 0.035	0.403 ± 0.110	0.288 ± 0.463	2.30	0.028
22	13.2	0.506 ± 0.043	0.503 ± 0.071	0.212 ± 0.065	0.356 ± 0.082	0.68	0.021

* One data point used in average.
H-pol—horizontal polarization.
V-pol—vertical polarization.

precipitation was present as detected from surface observations and the Grody (1991) method. All cases were determined to be overcast based on the ground LWP observations, with the exception of cases 14 and 16, which consisted of significant broken cloudiness. As in the clear-sky retrievals, the average cloudy-sky retrievals are based on the four SSM/I pixels nearest to Platteville. The ground observations were also averaged over a 1-h period centered on the satellite overpass time. While the length of time over which to average these data is somewhat arbitrary, it was thought that the 1-h average best represented the cloud conditions immediately surrounding the Platteville site.

The results of the retrievals from each method are shown in Table 3. Reasonable magnitudes of cloud LWP can be seen for the SC methods, although convergent solutions in the retrievals could not be found for all four pixels for case 8. However, upon comparison to the ground observations there are a few notable differences. For instance, in cases 16 and 20 the SC methods greatly overestimate the cloud LWP. The cause of these overestimations is not clear but may be related to an incorrect specification of the skin temperature or, possibly, effects on the surface emissivity from fairly recent rain events.

Another example of even greater interest is case 22. Here, the SC methods greatly underestimate the cloud LWP as compared to the ground observations. This case is unusual in that upslope conditions were present, creating a dense layer of low- to midlevel clouds from 680 mb to about 500 mb (the surface pressure was 843 mb). The reason for the poor retrievals is clear by referring back to the theoretical results shown in Fig. 8. The relationship between the 85.5-GHz T_b's and cloud LWP for case 22 resembles the midlatitude winter atmosphere but is offset about 7 K higher. As can be seen, the small response to cloud LWP results in two different cloud LWP values for a given T_b. Because of this ambiguity, the solution closest to the clear-sky T_b will be selected and thus underestimate the true cloud LWP. Also, the higher retrieved value for the H polarization as opposed to the V polarization can be explained by the larger brightening effect at H polarization.

As predicted from theory in Fig. 10, the NPD method should yield reasonable estimates of cloud LWP even in the presence of low clouds. The NPD method indeed provides a far better estimate of the cloud LWP than the SC methods for case 22 (Table 3). The extremely close agreement with the ground observations for this case is perhaps fortuitous; however, the errors in these retrievals are expected to be large for high amounts of cloud LWP because of the reduced sensitivity of ΔT_{85} to CLW under these conditions (see Fig. 10a).

In general, the NPD method performs remarkably well when compared to the ground observations. This success is due mainly to the higher than average surface polarization differences near Platteville, which produced fairly large clear-sky values of ΔT_{85} (greater than 2 K) and thus provided a sufficiently large cloud signal from which to retrieve cloud LWP. When the cloud LWP is low ($<$0.1 kg m^{-2}), as determined from the ground observations, the NPD method usually produces low LWPs, although there are exceptions. For instance, the retrievals slightly overestimate the cloud LWP for cases 16 and 20, but for case 16 the standard deviation is also very high, being comparable to the average. These are the same two cases where the SC method significantly overestimated the cloud LWP. This suggests the failure of both methods to retrieve low-cloud LWP for these cases might be related to the effects of surface moisture on the surface emissivities. Lastly, the NPD method also compares well to the ground observations for moderate values of cloud LWP (0.1–0.3 kg m^{-2}), as seen for cases 4, 8, and 9.

8. Conclusions and future work

A new method based on a normalized polarization difference has been developed to retrieve cloud LWP for nonprecipitating clouds over land surfaces using the 85.5-GHz channels of the SSM/I and IR measurements. A polarization difference approach can be applied over land surfaces since many land surfaces exhibit a small polarization signal. The method has the distinct advantages of being very insensitive to the surface skin temperature and is dependent only on the relative accuracy of the brightness temperatures rather than their absolute

accuracy. Also, this method has the ability to estimate cloud LWP for low-lying clouds, which is more difficult for the single-channel methods, as shown from theory and observational evidence. The NPD method is shown to be less useful in atmospheres with an abundance of water vapor and for large values of cloud LWP. However, based on theoretical simulations, the polarization difference at 37 GHz may also prove useful for retrieving cloud LWP under these conditions.

Composites of microwave surface emissivity over a 7-day period were used to represent the surface emissivity at the time of the satellite overpass for cloudy conditions. Through comparisons of forward model calculations with SSM/I observations in clear skies it is found that these composites are highly stable for most regions (rms errors of about 2.5 K) and thus can be reliably used as a background emissivity in the cloud LWP retrievals. Further comparison of the polarization difference of the brightness temperatures indicates that NPD retrievals of cloud LWP based on these 7-day composites are only possible when the clear-sky polarization difference is greater than about 1 K.

Preliminary comparisons of the NPD retrievals to a limited set of ground measurements are very encouraging. The method has demonstrated a reasonable amount of skill in at least discriminating between low, moderate, and high values of cloud LWP, which was principally a result of the surface polarization differences at the Platteville site being higher than average. The SC methods also do well in certain cases but at times are susceptible to large errors. Further testing of these methods will have to await more extensive validation efforts, which will be the subject of a future study. While the NPD method appears to perform better overall than the SC methods for the region near Platteville, it is anticipated that the best approach in retrieving cloud LWP over land surfaces in general will incorporate both types of methods.

A drawback of the retrieval methods described in this study is that they rely directly on additional information from surface and radiosonde observations. In the future it may be possible to develop a multisensor approach that is less dependent on these types of observations. The method might incorporate measurements from other sensors that also fly on the DMSP satellites, including the Special Sensor Microwave Temperature Sounder and the Special Sensor Microwave Water Vapor Sounder.

In terms of aircraft icing applications, we stress that although it may be possible to implement the cloud LWP retrievals on an operational basis there is the more serious problem of the limited temporal sampling of near-polar-orbiting satellites. These satellites only provide at best two overpasses a day over a specific region. However, a passive microwave instrument (that preferably measures dual polarization) aboard a geostationary platform would solve many of the temporal sampling problems. More frequent sampling would also make possible surface emissivity composites over shorter time periods, which may enhance the ability of the NPD method to retrieve cloud LWP under certain conditions.

Acknowledgments. We extend our thanks to Jack Snider at the NOAA Environmental Technology Laboratory in Boulder, Colorado, for providing the ground-based microwave radiometer data. The suggestions from two anonymous reviewers also helped to improve the paper. This study was funded by the Department of Defense under Contract DAAH04-94-G0420.

REFERENCES

Alishouse, J. C., J. B. Snider, E. R. Westwater, C. T. Swift, C. S. Ruf, S. A. Snyder, J. Vongsathorn, and R. R. Ferraro, 1990: Determination of cloud liquid water content using the SSM/I. *IEEE Trans. Geosci. Remote Sens.*, **28,** 817–821.

Diak, G. R., 1995: Column cloud liquid water amounts for nonprecipitating clouds versus an ''effective cloud fraction'' derived from microwave data: A simulation study. *J. Atmos. Oceanic Technol.,* **12,** 960–969.

Eyre, J. R., 1990: The information content of data from satellite sounding systems: A simulation study. *Quart. J. Roy. Meteor. Soc.,* **116,** 401–434.

Fowler, L. D., D. A. Randall, and S. A. Rutledge, 1996: Liquid and ice cloud microphysics in the CSU general circulation model. Part I: Model description and simulated microphysical processes. *J. Climate,* **9,** 489–529.

Greenwald, T. J., G. L. Stephens, T. H. Vonder Haar, and D. L. Jackson, 1993: A physical retrieval of cloud liquid water over the global oceans using Special Sensor Microwave/Imager (SSM/I) observations. *J. Geophys. Res.,* **98,** 18 471–18 488.

——, ——, S. A. Christopher, and T. H. Vonder Haar, 1995: Observations of the global characteristics and regional radiative effects of marine cloud liquid water. *J. Climate,* **8,** 2928–2946.

Grody, N. C., 1991: Classification of snow cover and precipitation using the Special Sensor Microwave Imager. *J. Geophys. Res.,* **96,** 7423–7435.

Hogg, D. C., F. O. Guiraud, J. B. Snider, M. T. Decker, and E. R. Westwater, 1983: A steerable dual-channel microwave radiometer for measurement of water vapor and liquid in the troposphere. *J. Climate Appl. Meteor.,* **22,** 789–806.

Hollinger, J. P., R. Lo, G. Poe, R. Savage, and J. Peirce, 1987: *Special Sensor Microwave/Imager User's Guide,* Naval Research Laboratory, 120 pp.

——, J. L. Peirce, and G. A. Poe, 1990: SSM/I instrument evaluation. *IEEE Trans. Geosci. Remote Sens.,* **GE-28,** 781–791.

Huang, H.-L., and G. R. Diak, 1992: Retrieval of nonprecipitating liquid water cloud parameters from microwave data: A simulation study. *J. Atmos. Oceanic Technol.,* **9,** 354–363.

Jones, A. S., 1996: The use of satellite-derived heterogeneous surface soil moisture for numerical weather prediction. Ph.D. dissertation, Colorado State University, 520 pp.

——, and T. H. Vonder Haar, 1990: Passive microwave remote sensing of cloud liquid water over land regions. *J. Geophys. Res.,* **95,** 16 673–16 683.

——, K. E. Eis, and T. H. Vonder Haar, 1995: A method for multisensor–multispectral satellite data fusion. *J. Atmos. Oceanic Technol.,* **12,** 739–754.

Koch, S. E., M. desJardins, and P. J. Kocin, 1983: An interactive Barnes objective map analysis scheme for use with satellite and conventional data. *J. Climate Appl. Meteor.,* **22,** 1487–1503.

Lee, T. F., J. R. Clark, and S. D. Swadley, 1994: Potential applications of the SSM/I cloud liquid water parameter to the estimation of marine aircraft icing. *Wea. Forecasting,* **9,** 173–182.

Liebe, H. J., 1989: MPM—An atmospheric millimeter wave propagation model. *Int. J. Infrared Millimeter Waves,* **10,** 631–650.

——, G. A. Hufford, and M. G. Cotton, 1993: Propagation modeling of moist air and suspended water/ice particles at frequencies below 1000 GHz. *Proc. Atmospheric Propagation Effects through Natural and Man-Made Obscurants for Visible to MM-Wave Radiation,* Palma de Mallorca, Spain, AGARD, 3.1–3.10.

McClatchey, R. A., R. W. Fenn, J. E. Selby, F. E. Voltz, and J. S. Garing, 1972: Optical properties of the atmosphere. 3d. ed. AFCRL Environmental Research Paper 411, 108 pp. [Available from Air Force Cambridge Research Laboratories, L. G. Hanscom Field, Bedford, MA 01731.]

McMillin, L. M., and H. E. Fleming, 1976: Atmospheric transmittance of an absorbing gas: A computationally fast and accurate transmittance model for absorbing gases with constant mixing ratios in inhomogeneous atmospheres. *Appl. Opt.,* **15,** 358–363.

Minnis, P., and E. F. Harrison, 1984: Diurnal variability of regional cloud and clear-sky radiative parameters derived from GOES data. Part I: Analysis method. *J. Climate Appl. Meteor.,* **23,** 993–1001.

Petty, G. W., 1990: On the response of the Special Sensor Microwave/Imager to the marine environment—Implications for atmospheric parameter retrievals. Ph. D. dissertation, University of Washington, 291 pp.

Spencer, R. W., H. M. Goodman, and R. E. Hood, 1989: Precipitation retrieval over land and ocean with the SSM/I: Identification and characteristics of the scattering signal. *J. Atmos. Oceanic Technol.,* **6,** 254–273.

Tjemkes, S. A., G. L. Stephens, and D. L. Jackson, 1991: Spaceborne observation of columnar water vapor: SSMI observations and algorithm. *J. Geophys. Res.,* **96,** 10 941–10 954.

Wielicki, B. A., R. D. Cess, M. D. King, D. A. Randall, and E. F. Harrison, 1995: Mission to planet earth: Role of clouds and radiation in climate. *Bull. Amer. Meteor. Soc.,* **76,** 2125–2153.

Zuidema, P., and D. L. Hartmann, 1995: Satellite determination of stratus cloud microphysical properties. *J. Climate,* **8,** 1638–1657.